Brain Stimulation 16 (2023) 1154–1164

Contents lists available at ScienceDirect

Brain Stimulation

journal homepage: www.journals.elsevier.com/brain-stimulation

Transcranial direct current stimulation elevates the baseline activity while sharpening the spatial tuning of the human visual cortex

Jeongyeol Ahn [a], Juhyoung Ryu [a], Sangjun Lee [b], Chany Lee [c], Chang-Hwan Im [d], Sang-Hun Lee [a,*]

[a] Department of Brain and Cognitive Sciences, Seoul National University, Seoul, Republic of Korea
[b] Department of Biomedical Engineering, University of Minnesota, Minneapolis, MN, USA
[c] Department of Structure & Function of Neural Network, Korea Brain Research Institute, Daegu, Republic of Korea
[d] Department of Biomedical Engineering, Hanyang University, Seoul, Republic of Korea

1. Introduction

Early studies on animal brains [1,2] have suggested that surface-positive and negative currents elevate and suppress neuronal excitability, respectively. These effects lasted for several minutes to hours after the stimulation was switched off. However, the effects of transcranial direct current stimulation (tDCS) on human brains have been inconsistent. Some studies have reported polarity-specific modulation of excitability in the motor domain, but recent studies has found significant effects only with anodal-tDCS (a-tDCS) and not with cathodal-tDCS (c-tDCS) [3]. This asymmetry has also been observed in other domains, with upregulation by a-tDCS often significant and downregulation by c-tDCS scarcely significant [4].

The inconsistency seen in tDCS on human brains may be due to various factors. Firstly, the effectiveness of tDCS may vary depending on the structural or functional properties of the neural system it is applied to [5–7]. For example, modeling work suggests that both excitatory pyramidal cells and inhibitory interneurons should be considered to explain tDCS effects sufficiently [8]. This means that tDCS may produce different outcomes depending on the balance between excitatory and inhibitory neurons in a given neural system, which is plausible given the substantial variation in excitatory-inhibitory balance throughout the brain [9]. Secondly, individual differences such as brain and skull morphology, neurotransmitter composition, and genetic profile [6,7] may also contribute to the inconsistency. For example, the electric-field differences owing to skull and brain anatomies [9,10] or neurotransmitter efficiency [11] accounted for the across-individual variability of tDCS effects. Lastly, poor experimental designs may also lead to inconsistency. Any failure in controlling the various within-day and across-day noises and in making both subjects and experimenters blind to stimulation conditions may mask subtle, modulatory tDCS effects [5,12].

Given the above factors contributing to the inconsistency of tDCS effects on human brains, it is required to investigate tDCS effects on diverse brain regions while implementing tight experimental controls and statistical analyses to address individual differences. For this purpose, we used functional magnetic resonance imaging (fMRI) to measure blood-oxygenation-level-dependent (BOLD) responses to dynamic visual patterns from the human early visual cortex (EVC) while simultaneously stimulating it with tDCS. To effectively address the issues mentioned above, we have incorporated the following points into the design of our experiment.

First, there are several reasons to select EVC as a target brain region. The well-known functional architecture of EVC, such as retinotopic representations by neurons with receptive fields [13–16], allows us to estimate various system-level changes of cortical activity using fMRI. With such a refined assessment of tDCS effects, we expect to gain valuable insights into how it affects cortical activity at a functional level. We also considered the fact that EVC has been less studied in previous tDCS research, particularly in comparison to the motor cortex [17–22]. Given the substantive differences in biophysical properties between EVC and the motor cortex [23,24], including the difference in the excitatory-vs-inhibitory (E/I) balance of recurrent circuits, the impact of tDCS on EVC may differ from that found in the motor cortex. Such differential impacts would provide fruitful clues for how tDCS affects cortical activity at a circuit level. Second, to create an ideal electric field in EVC, we used a multi-electrode tDCS system in conjunction with a high-fidelity stimulation protocol. Specifically, to address the across-subject differences due to skull and brain morphology, we tuned stimulation protocols using the electric field simulation carried out on the individual head anatomies. This approach allowed us to deliver effective stimulation tailored to each individual. Lastly, we adopted a sham-controlled crossover design, such that each subject participated in all three types of the daily session—the 'anodal,' 'cathodal,' and 'sham'

* Corresponding author.
E-mail addresses: aeolian@snu.ac.kr (J. Ahn), visionsl@snu.ac.kr (S.-H. Lee).

https://doi.org/10.1016/j.brs.2023.07.052
Received 8 February 2023; Received in revised form 4 June 2023; Accepted 23 July 2023
Available online 28 July 2023

sessions. All sessions shared an identical structure, acquiring BOLD responses before (pre-stimulation), during (during-stimulation), and after (post-stimulation) stimulation. This design corrects the BOLD responses in the four main experimental conditions (2 stimulation polarities x 2 stimulation phases) for the tDCS-irrelevant fluctuations in BOLD signal known to occur within a daily session and between daily sessions or individuals.

We assessed the tDCS effects on EVC for the following aspects. We inspected the temporal dynamics of the BOLD responses to a transient full-field visual pattern to see whether tDCS perturbs the transient or sustained neural activity or the neuro-vascular function. We also inspected the spatial tuning of EVC using traveling-wave visual patterns [25–29]. Changes in pRF would inform us of the cortical mechanism that mediates tDCS effects, such as the surround inhibition or long-range facilitation mechanisms known to modulate the spatial tuning of visual neurons [30–33]. We also analyzed the noise correlation between cortical sites, which is known to play a crucial role in information processing as demonstrated by computational [34], animal electrophysiological [35], and human fMRI studies [36–38].

We found that a-tDCS elevated the baseline, but not stimulus-driven, cortical activity while sharpening the spatial tuning by augmenting surround suppression in EVC. These findings are at odds with the previous findings reported on the motor cortex, suggesting that tDCS effects on the visual cortex might differ from those reported in the motor cortex.

2. Methods

2.1. Subjects

Fifteen subjects (two authors included) with a mean age of 25.7 ± 4.17 years (five females) contributed to the dataset for analysis (see Supplementary materials for details). All subjects had normal or corrected-to-normal vision. They all provided written informed consent. All procedures complied with the safety guidelines and standards approved by the Institutional Review Board of Seoul National University (1711/003–027).

2.2. Experimental design: sham-controlled crossover experimental design with double blinds

Each subject participated in four daily sessions: retinotopy-mapping, a-tDCS, c-tDCS, and sham-tDCS sessions, which were randomized in order across subjects and separated from one another by at least a week to ensure a sufficient washout of the preceding effects. In each session a pre-stimulation phase was followed by peri-stimulation and post-stimulation phases, which are all identical in fMRI scan structure, each consisting of one temporal-profile scan and four spatial-profile scans (Fig. 1b). The genuine tDCS was applied only in the 'peri-stimulation' phase of the a-tDCS and c-tDCS sessions.

2.3. tDCS protocol

We applied tDCS using the Starstim tES 8-channel system with a multi-channel MRI extension kit. The system was remotely controlled by the software Neuroelectrics Instrument Controller (NIC2). Eight saline-soaked circular sponges (8 cm^2) with carbon rubber electrodes were arranged to form a center-surround geometry on the surface of the head (Fig. 1d). The total amount of electric current was set to 2 mA. The electrode arrangement and current amount were identical for a-tDCS and c-tDCS: only the direction of the current was reversed. The durations

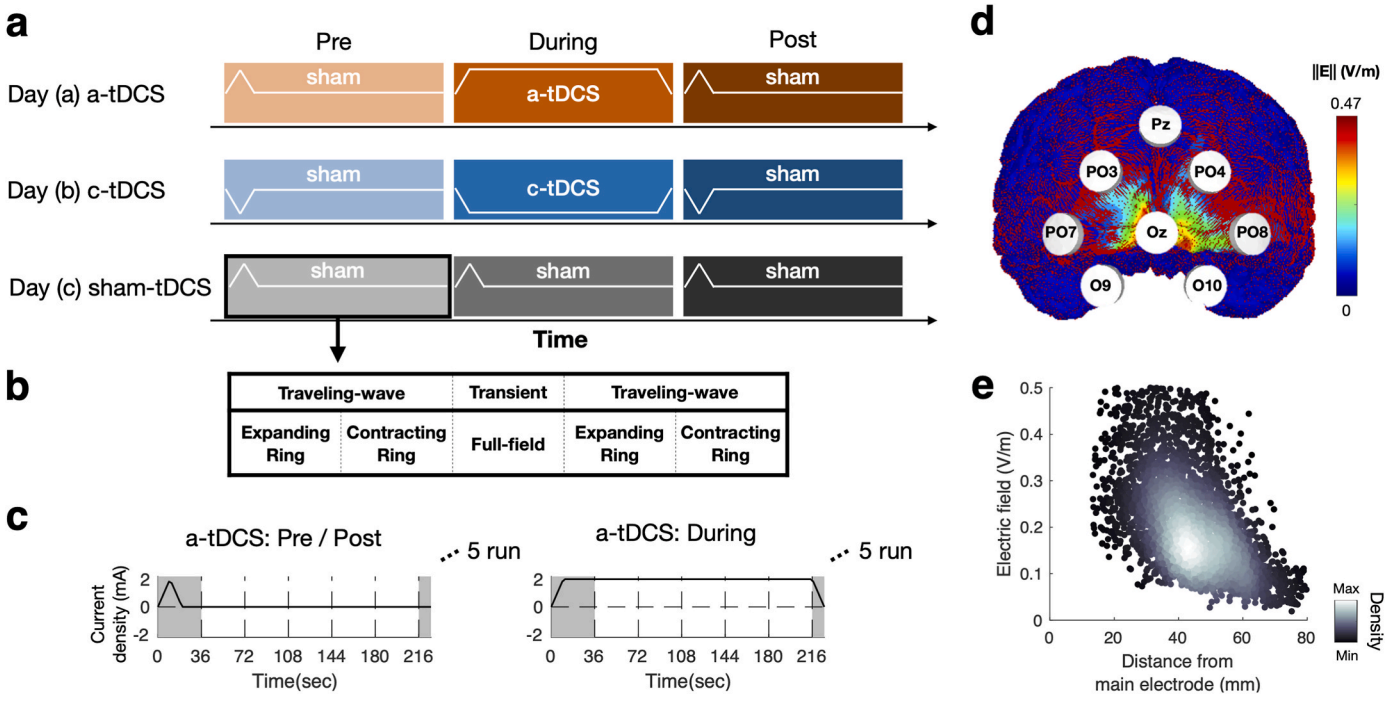

Fig. 1. Design of tDCS-fMRI experiment and tDCS montage.
(a) Sham-controlled crossover design. Each subject participated in the anodal (a-tDCS), cathodal (c-tDCS), and sham (sham-tDCS) tDCS sessions on three different days. Each session consisted of three stimulation phases, one before (pre), one during (during), and the other after (post) the stimulation. (b) Structure of scan runs. Each stimulation phase consisted of five scan runs, four devoted to pRF mapping based on the traveling-wave input and the other to temporal profile mapping based on the transient full-field input. (c) Time courses of electric current. Two general types of electric stimulation were used (see the white line curves in a): the one used in pre- or post-stimulation phases and the other in during-stimulation phases. In the former, the current was switched on and quickly off as a control for placebo effects. In the latter, the current was switched on and maintained throughout the entire run. We discarded the BOLD data acquired during the first cycle in which the "fake-stimulation" was applied (demarcated by gray regions). (d) Eight-channel tDCS montage and an example electric field simulation shown for one subject. (e) Density plot of electric field density distribution estimated from simulation for all voxels.

of ramping-up and ramping-down electric current were set to 10 s each (Fig. 1c). Each subject received a total of 18-min long (5 runs × 216 s) genuine tDCS in both a-tDCS and c-tDCS sessions.

2.4. Optimization of the pattern of injection current for individuals

To benefit maximally from the multi-channel tES system's focal stimulation, it is crucial to optimize the injection current pattern for each individual's brain. To do this, we first constructed a sophisticated 3D finite element (FE) head model for each brain, consisting of five tissue components (white matter, gray matter, cerebrospinal fluid, skull, and scalp). We constructed the FE head models from T1-weighted MR images using a series of software packages, including SimNIBS, FreeSurfer, and FSL [39–41]. We then virtually attached eight circular sponge electrodes to the scalp surface of the FE head models, at Oz, PO7, PO8, PO3, PO4, Pz, O9, and O10, according to the extended 10–20 EEG placement system [42]. Next, we analyzed an electric field by applying the finite element method (FEM) to each FE head model to determine the optimal injection current pattern that maximizes the electric field flowing into our target ROI, V1, with an evolutionary strategy (see "Electric field simulation to optimize tDCS for individuals" section of the supplementary materials for further details).

2.5. fMRI data preprocessing

The images acquired across different sessions and runs were aligned to the high-resolution T1 images based on the T1 images (see Supplementary materials for details) using SPM8 (http://fil.ion.ucl.ac.uk/spm) and mrTools (http://cns.nyu.edu/heegerlab/?page=software). The first-cycle data of each run were discarded for fMRI signal stabilization, so the images acquired during the brief stimulation period in the sham scan runs were not included in the data analysis (Fig. 1c).

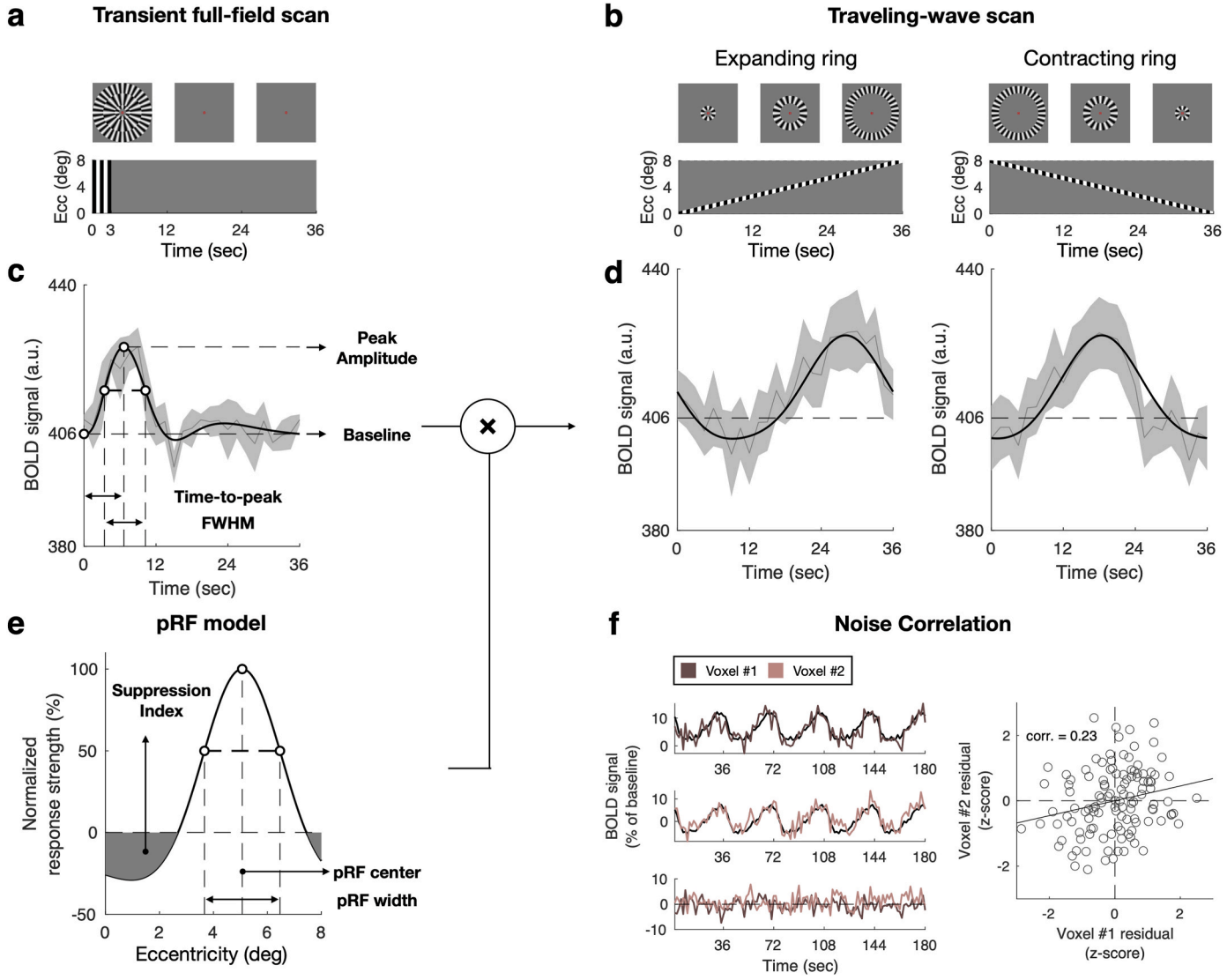

Fig. 2. Quantification of temporal and spatial profiles of BOLD responses.
(a-b) Stimuli and paradigm for characterizing the spatial and temporal profile of BOLD responses to transient full-field (a) and traveling-wave (b) input. (c–d) Example one-cycle averages of a single voxel's BOLD responses to the transient full-field (c) and traveling-wave (d) input. The model time series (black curves) was fit to the observed ones (gray curves). The shades demarcate the across-cycle standard deviation. The dashed lines and arrows indicate the temporal-profile measures in c. (e) Example difference-of-Gaussian model of pRF with three parameters fit to the single voxel's BOLD responses to the traveling-wave input depicted in d. The dashed lines and arrows indicate the pRF measures. (f) Quantification of noise correlation. Left, the process of extracting noise time series shown for two example voxels. Noise time series were defined by subtracting the concatenated across-cycle averages of BOLD responses from the raw BOLD time series. Right, definition of noise correlation. The noise time points of one of the two voxels depicted in the left panel are plotted against those of the other voxel. (For interpretation of the references to color in this figure legend, the reader is referred to the Web version of this article.)

2.6. Temporal-profile analysis of BOLD responses to transient full-field input

In each 36-s cycle, sinusoidal radial gratings were presented within a large (8° in radius) circular aperture for 3 s and then disappeared for 33 s (Fig. 2a). We fit the hemodynamic impulse response function (HIRF) with the two gamma functions [43] to each voxel's time series of BOLD responses by predicting the time series based on the convolution of the stimulus event matrix with the HIRF. From the best-fit predicted time course of BOLD responses, we defined 'baseline' as the predicted BOLD response at stimulus onset; 'peak amplitude' as the fractional change from the BOLD value at stimulus onset to that at peak (i.e., $(BOLD_{peak} - BOLD_{onset})/BOLD_{onset}$); 'Time to peak' as the time taken for BOLD responses to reach the peak; 'FWHM' as the time taken to reach its second half-of-maximum value after it reached its first half-of-maximum value (Fig. 2c).

2.7. Spatial-profile analysis of BOLD responses to traveling-wave input

In each 36-s cycle, sinusoidal radial gratings presented within ring-shape apertures slowly (4.5 v.a.d./sec) traversed the visual field in the radial direction (Fig. 2b). With the 1D difference-of-Gaussian (DoG) function [44], pRF was defined as a gain function ($g(x)$) of stimulus input (x) as follows:

$$g(x) = \beta_+ g_+(x) - \beta_- g_-(x);$$

$$g_+(x) = \exp - \left(\frac{(x-x_0)^2}{2{\sigma_+}^2}\right);\ g_-(x) = \exp - \left(\frac{(x-x_0)^2}{2{\sigma_-}^2}\right), \quad (6)$$

where $g_+(x)$ and $g_-(x)$ are positive and negative Gaussian functions, the respective contributions of which to $g(x)$ are expressed by the two coefficients, β_+ and β_-; x_0 is the center of pRF, and σ_+ and σ_- are the standard deviations of the positive and negative Gaussian functions, respectively. Next, we predicted the aggregated responses of a population of visual neurons within a voxel to the traveling-wave input ($r(t)$) by convolving a binary matrix of spatiotemporal stimulus input ($s(x, t)$) with $g(x)$ (Fig. 2c–e). Finally, we predicted the BOLD responses by convolving $r(t)$ with the HIRF defined by the transient-stimulus scan in each stimulation phase. From the best-fit pRF defined above, we defined 'pRF center' as the pRF parameter x_0; 'pRF width' as the FWHM of the positive part of pRF; 'pRF SI' as the ratio of the integration of the negative part of pRF to the integration of the positive part of pRF within the visual field of interest (0–8 v.a.d. in eccentricity) (Fig. 2e).

2.8. Noise correlation estimation

We extracted the noise time series for each voxel by repeatedly concatenating the across-cycle average response to match the scan run length and subtracting it from the original BOLD. Then, Pearson's correlation coefficient between two noise time series was computed for all possible pairs of voxels (Fig. 2f). Then, we averaged the Fisher's z-transformed correlation coefficients [45] across all possible voxel pairs that include a single voxel of interest as follows:

$$z_{N.C.} = \sum_{\substack{i=1 \\ i \neq j}}^{n} F(r_{i,j}) \Big/ n-1, \quad (7)$$

where $F(r) = tanh^{-1}(r)$ and $r_{i,j}$ is a Pearson's correlation coefficient in noise time series between voxel i and j.

2.9. Statistical analysis

We evaluated the statistical significance of tDCS effects, as follows: (1) the measures obtained in the pre-stimulation phase were subtracted from those obtained in the during-stimulation and post-stimulation phases to control for tDCS-irrelevant variability in BOLD activity across daily sessions; (2) we evaluated whether (1) differ from 'the corresponding subtracted measures of the sham-tDCS daily session' to control for tDCS-irrelevant fluctuations of BOLD responses over time within single daily sessions. Specifically, for each measure, this evaluation was carried out using two mixed-effect ANOVA models, one for a-tDCS and the other for c-tDCS, because the polarity effects might not be symmetric [4]. See the supplementary materials for how we carried out the two robustness tests.

2.10. Time course analysis of tDCS effects on the baseline, time-to-peak, and spatial-tuning measures of BOLD responses

Measurement. As for the baseline, we averaged the raw BOLD responses within each scan for each voxel. As for the time-to-peak, we fitted the sine function to the cycle-averaged BOLD time series. Then the phase value of the sine function was converted into the time unit ($2\pi : 36\ sec$). As for the pRF width and pRF SI, we fitted the DoG function to the pair of traveling-wave scan runs, one traveling inward and the other outward.

Linear regression analysis. We did a linear regression analysis to test whether tDCS effects gradually increase or decrease during the during-stimulation phase. We set 0 to regressors for pre-stimulation runs, [0.1, 0.3, 0.5, 0.7, 0.9] for during-stimulation runs, and then 1 for post-stimulation runs so that we can interpret the slope of the regression as a degree of linear change during the stimulation.

2.11. Voxel selection for illustrative summary

We selected voxels with four criteria based on only the a-tDCS session data. First, the baseline parameter increased in the post-stimulation phase compared with pre-stimulation. Second, time-to-peak increased in during-stimulation compared with pre-stimulation. Third, pRF width decreased in post-stimulation compared with pre-stimulation. Fourth, pRF SI increased in post-stimulation compared with pre-stimulation. 11% of voxels passed such criteria.

3. Results

3.1. Initial statistical results

In the during-stimulation phase, a-tDCS affected only the temporal dynamics of BOLD responses to the transient visual input, decreasing the 'peak amplitude' ($Z = -4.60$, FDR-adjusted $p < 1.E{-}05$) and increasing the 'time-to-peak' ($Z = 4.28$, FDR-adjusted $p < 1.E{-}04$) and the 'FWHM' ($Z = 3.34$, FDR-adjusted $p < 1.E{-}02$) of the BOLD time series (Fig. 3a). By contrast, no measure was affected by c-tDCS (Fig. 3b).

During the post-stimulation phase, many of the BOLD measures were significant. Specifically, a-tDCS increased the baseline ($Z = 7.38$, FDR-adjusted $p < 1.E{-}11$), decreased the 'peak amplitude' ($Z = -2.01$, FDR-adjusted $p < 0.05$), reduced the pRF width ($Z = -5.19$, FDR-adjusted $p < 0.01$), increased the pRF SI ($Z = 4.47$, FDR-adjusted $p < 0.01$), and decreased the noise-correlation ($Z = -12.90$, FDR-adjusted $p < 0.05$) (Fig. 3c). On the other hand, c-tDCS decreased the 'FWHM' ($Z = -4.60$, FDR-adjusted $p < 0.05$), increased the 'pRF center' ($Z = 2.33$, FDR-adjusted $p < 0.05$), decreased the 'pRF width' ($Z = -5.19$, FDR-adjusted $p < 0.05$), and decreased the noise-correlation measure ($Z = -12.90$ FDR-adjusted $p < 0.01$) (Fig. 3d).

Table 1 shows the detailed results of all (32 tests = 8 measures x 2 polarity x 2 stimulation phases) mixed-effect ANOVA tests.

3.2. Evaluating the robustness of the initial statistical results

We assessed the robustness of the above significant effects by

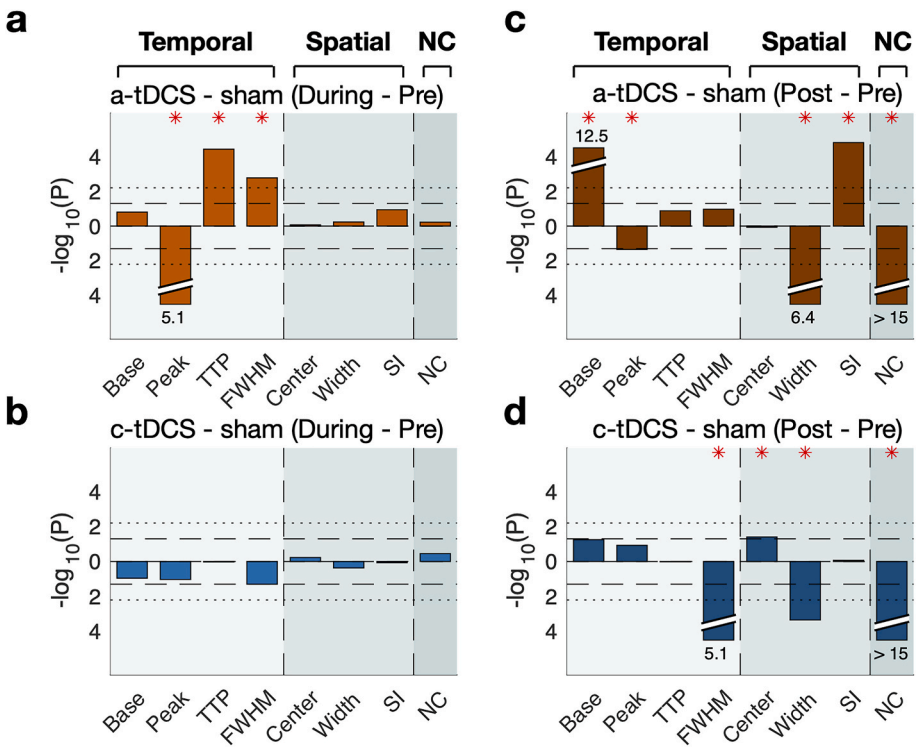

Fig. 3. Initial statistical results.
(a-d) Modified Manhattan plots of mixed-effect ANOVA tests for the a-tDCS/during-stimulation (a), c-tDCS/during-stimulation (b), a-tDCS/post-stimulation (c), and c-tDCS/post-stimulation (d) effects. The signed (+, increase; -, decrease) log of P values of the mixed-effect ANOVA tests are plotted against the temporal-profile (light teal background), spatial-profile (teal background), and noise-correlation (dark teal background) measures. Horizontal dashed and dotted lines demarcate the significance level with and without Bonferroni correction, respectively. Red stars mark the measures with significant (FDR-adjusted $p < 0.05$) tDCS effects. (For interpretation of the references to color in this figure legend, the reader is referred to the Web version of this article.)

inspecting how reliably they retain statistical significance across different subpopulations of voxels or subjects. Such assessment is crucial in tDCS experiments on human subjects because the tDCS effects on human brains can be variable in both magnitude and direction across local sites and subjects, although our tDCS stimulation protocols were optimized to the head anatomy of each subject.

First, we considered an imperfect alignment between daily sessions as the source of the across-voxel variability in tDCS effects. Using the between-session correlation in the BOLD time series during the pre-stimulation phase as a proxy of voxel correspondence, we refined the pool of valid voxels with varying levels of voxel correspondence. Then, we repeated the mixed-effect ANOVA test on those refined pools. Three of the initially significant results failed to survive this test (red symbols in Fig. 4c and d).

Next, to assess the robustness of the statistical test outcomes to the subject-wise variability, we inspected whether the data set from a single 'influential' subject determined the statistical results using the jackknife resampling technique (Fig. 5). Seven of the initially significant outcomes failed to survive this test of robustness to subject-wise variability (red symbols in Fig. 5a,c,d).

By putting the initially significant tDCS effects to the two robustness tests, we found that only the anodal application of tDCS "reliably" modulated (i) the 'time-to-peak' measure of BOLD responses to the transient stimuli during the during-stimulation phase, (ii) the 'baseline' measure of BOLD responses to the transient stimuli during the post-stimulation phase, and (iii) the 'pRF width' and 'pRF SI' measures of BOLD responses to the traveling-wave stimuli during the post-stimulation phase. In what follows, to see how these effects temporally develop, we probed the BOLD responses on a run-to-run basis.

3.3. Time course of tDCS effects on BOLD baseline, time-to-peak, and pRF shape

For this run-to-run inspection, we acquired the baseline and time-to-peak measurements using the methods that can be applied not only to the BOLD responses to the transient visual input but also to those to the traveling-wave input (see Methods for details). We found that the baseline measures steadily grew while a-tDCS was applied and remained high after switching off the stimulation (red symbols and lines in Fig. 6a). We did not find such a gradual elevation in the c-tDCS (blue symbols and lines in Fig. 6a) or the sham-control conditions (gray symbols and lines in Fig. 6a).

As for the time-to-peak measures, we fitted the sine function to the BOLD time series of each scan run by capitalizing on the fact that the transient and traveling-wave inputs share the same periodic cycle (see Methods for details). We did not find any trend in these time-to-peak measures—neither increase nor decrease—regardless of the tDCS stimulation conditions (Fig. 6b).

In principle, the spatial-tuning (i.e., pRF) measures cannot be estimated from the BOLD responses to the transient visual input. In addition, the reliable pRF estimation requires the pair of traveling-wave scan runs, one traveling inward and the other outward. Thus, we acquired the spatial-tuning measures by fitting the pRF model to the BOLD time series in the two contiguous traveling-wave runs, which resulted in the six points of pRF width and pRF SI measures. The pRF-width and pRF-SI measures tended to decrease and increase, respectively, while a-tDCS was applied and remained high and low, respectively, after a-tDCS was withdrawn (red symbols and lines in Fig. 6c, d).

In sum, from the moment of a-tDCS application, the BOLD responses steadily increased in baseline while their spatial-tuning function became narrow and suppressed in the surround.

3.4. Illustrative summary of tDCS effects

Having identified the significant and robust effects of tDCS on visual BOLD responses and analyzed their time courses, we conclude the Results section by providing an *illustrative* summary of those effects. This illustrative summary is needed because it is not easy to appreciate the effects due to their modulatory (subtle), idiosyncratic (variable across individuals), and noisy (variable across voxels) nature. For this illustrative purpose, we opted to "cherry-pick" a specific set of voxels (see Methods for details). With this "paragon" set of voxels, we illustrate (1) the tDCS effects on the baseline and time-to-peak measures by plotting their cycle-averaged BOLD responses to the transient visual input

Table 1
Initial statistical results from the planned comparison with Mixed ANOVA.

Param	tDCS	Comparison	Std. Error	Z-value	P-value	Significance
Base	a-tDCS	a-tDCS - sham (During - Pre)	0.002	1.41	0.16	
		a-tDCS - sham (Post - Pre)	0.002	7.38	3. E−13	*
	c-tDCS	c-tDCS - sham (During - Pre)	0.002	−1.60	0.11	
		c-tDCS - sham (Post - Pre)	0.002	2.20	0.06	
Peak	a-tDCS	a-tDCS - sham (During - Pre)	0.001	−4.60	8. E−06	*
		a-tDCS - sham (Post - Pre)	0.001	−2.01	0.04	*
	c-tDCS	c-tDCS - sham (During - Pre)	0.001	−1.99	0.09	
		c-tDCS - sham (Post - Pre)	0.001	1.56	0.12	
TTP	a-tDCS	a-tDCS - sham (During - Pre)	0.141	4.28	4. E−05	*
		a-tDCS - sham (Post - Pre)	0.141	1.51	0.13	
	c-tDCS	c-tDCS - sham (During - Pre)	0.141	−0.72	0.94	
		c-tDCS - sham (Post - Pre)	0.141	−0.04	1. E+00	
FWHM	a-tDCS	a-tDCS - sham (During - Pre)	0.163	3.34	2. E−03	*
		a-tDCS - sham (Post - Pre)	0.163	1.61	0.11	
	c-tDCS	c-tDCS - sham (During - Pre)	0.161	−1.96	0.05	
		c-tDCS - sham (Post - Pre)	0.161	−4.60	0.00	*
Center	a-tDCS	a-tDCS - sham (During - Pre)	0.061	0.19	9. E−01	
		a-tDCS - sham (Post - Pre)	0.061	−0.68	0.85	
	c-tDCS	c-tDCS - sham (During - Pre)	0.057	0.54	0.59	
		c-tDCS - sham (Post - Pre)	0.057	2.33	4. E−02	*
Width	a-tDCS	a-tDCS - sham (During - Pre)	0.093	0.55	6. E−01	
		a-tDCS - sham (Post - Pre)	0.093	−5.19	0.00	*
	c-tDCS	c-tDCS - sham (During - Pre)	0.093	−0.79	0.43	
		c-tDCS - sham (Post - Pre)	0.093	−3.69	0.00	*
SI	a-tDCS	a-tDCS - sham (During - Pre)	0.011	1.58	1. E−01	
		a-tDCS - sham (Post - Pre)	0.011	4.47	0.00	*
	c-tDCS	c-tDCS - sham (During - Pre)	0.011	−0.19	0.85	
		c-tDCS - sham (Post - Pre)	0.011	0.75	9. E−01	
NC	a-tDCS	a-tDCS - sham (During - Pre)	0.002	0.53	6. E−01	
		a-tDCS - sham (Post - Pre)	0.002	−12.90	0.00	*
	c-tDCS	c-tDCS - sham (During - Pre)	0.002	0.93	0.35	
		c-tDCS - sham (Post - Pre)	0.002	−12.73	2. E−37	*

(Fig. 6e) and (2) the tDCS effects on the pRF width and SI measures by plotting the pRF profiles with the averaged-across-voxel parameters best-fit to the BOLD responses to the traveling-wave input (Fig. 6f).

From (1), we can readily appreciate the impact of a-tDCS on the raw cortical responses to the transient input: it shifts their entire time series upward while delaying its peak slightly. From (2), we understand how a-tDCS changes the spatial profile of pRF: it sharpens the spatial tuning by narrowing the width of the positive center while augmenting the suppression at the immediate surround. These plots must be taken not as representative (typical) results but as a selected sample of data for an illustrative purpose.

4. Discussion

To check how tDCS modulates cortical visual responses, we kept track of the spatial and temporal aspects of the BOLD activity of EVC before, during, and after tDCS application while varying the presence and polarity of tDCS application. We found that a-tDCS elevated the baseline BOLD activity without affecting the stimulus-driven activity while sharpening the voxels' spatial tuning profiles by augmenting surround suppression. These effects grew gradually from electrical stimulation onset till its offset and remained substantial afterward. We ascertained the robustness of these findings to the two well-known nuisance factors of electrical brain stimulation studies.

4.1. Buildup and persistence of a-tDCS effect on baseline BOLD activity

The current work found that the baseline BOLD activity gradually ramped up as the surface-positive current flowed into there and persisted for an extended period (at least 20 min) even after the current was switched off. Its magnitude was substantial, corresponding to 50% of the stimulus-driven BOLD activity (Fig. 6a). This ramping and persisting dynamics is strikingly similar to that in the seminal work by Bindman and her colleagues [1,46], where the authors showed that when the polarizing current was applied for a 5 min or longer period, the spontaneous firing rate of somatosensory neurons increased steadily as the current was applied and persisted at that elevated level after it was switched off.

To our knowledge, our study provides the first report on the impact of a-tDCS on the baseline BOLD activity in human brains. Given its substantial magnitude and persistence in our study, one might wonder why such an impact has never been discovered in previous tDCS-fMRI studies. We note that most tDCS-fMRI studies focused on measuring the stimulus- or task-evoked, which led them to adopt the widespread practice of normalizing raw BOLD time series within each single scan run. This practice precludes the opportunity to observe the gradual changes in baseline activity. We anticipate that our finding on the baseline BOLD will likely be replicated by previous or future tDCS-fMRI studies if raw BOLD time series are normalized over the entire fMRI session as we did.

4.2. Dissociation between baseline and stimulus-driven BOLD responses in tDCS effects on EVC

We did not observe any signs of ramping or persistence dynamics in the impact of a-tDCS on the BOLD responses to visual stimuli. The only effect induced by a-tDCS that was both significant and consistent was a slight delay in time-to-peak. However, this delay was brief, lasting only between 0.1 and 0.5 s, only noticeable during the stimulation phase in the transient input scan run, and not comparable to the effects of a-tDCS on the baseline BOLD activity in terms of magnitude and dynamics.

By contrast, previous studies on the human motor cortex showed that significant effects on task-driven BOLD responses could be achieved when sufficiently long (10–20 min) a-tDCS stimulations were applied to the motor cortex [17–20], unlike when relatively short stimulations (only 20 s or 5 min) were applied [20–22].

In a broad context, this contrast between these BOLD studies on the motor cortex and ours seems consistent with the view that the effects of tDCS might vary across different brain areas. For example, previous studies have shown that the surface-positive current modulated the

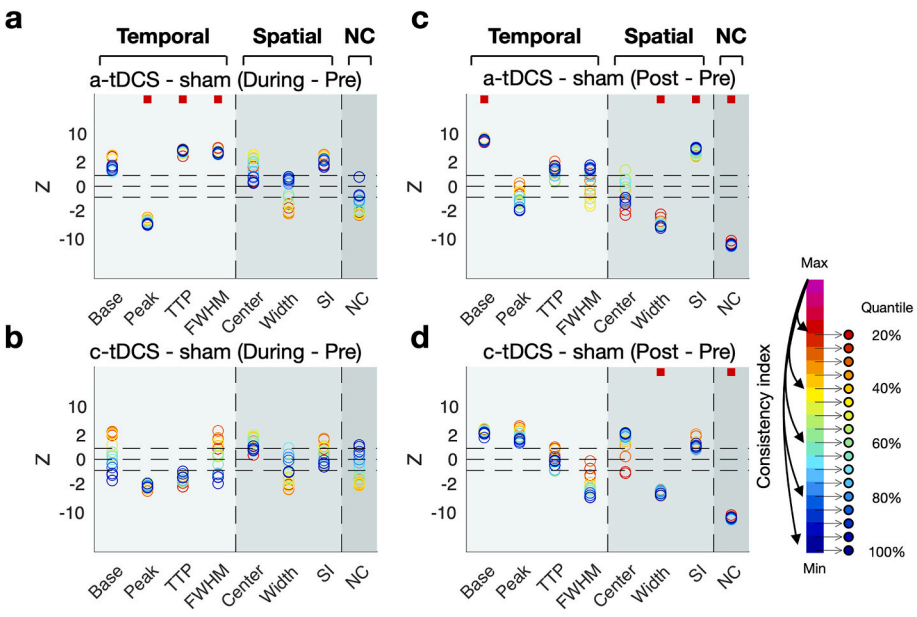

Fig. 4. Test results of robustness to voxel misalignment.
(a-d) Plots of robustness-to-voxel-misalignment test results for the a-tDCS/during-stimulation (a), c-tDCS/during-stimulation (b), a-tDCS/post-stimulation (c), and c-tDCS/post-stimulation (d) effects. The test statistics (Z; +, increase; -, decrease) are plotted against the temporal-profile (light teal background), spatial-profile (teal background), and noise-correlation (dark teal background) measures. Colors represent the quantiles of voxel-selection criteria for consistency index (equally spaced 17 bins from highest 20%–100% with a step size of 5%). Horizontal dashed lines demarcate the significance level. Red squares indicate that the test statistics were significant at all bins. (For interpretation of the references to color in this figure legend, the reader is referred to the Web version of this article.)

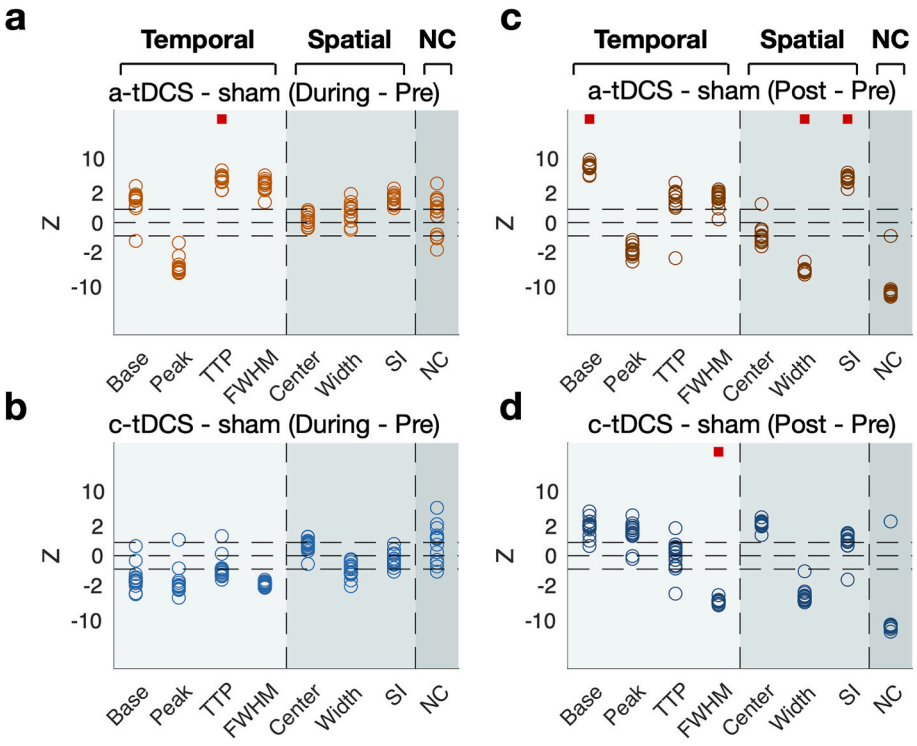

Fig. 5. Test results of robustness to inter-subject variability.
(a-d) Plots of robustness-to-inter-subject-variability test results for the a-tDCS/during-stimulation (a), c-tDCS/during-stimulation (b), a-tDCS/post-stimulation (c), and c-tDCS/post-stimulation (d) effects. The statistics (Z; +, increase; -, decrease) of the 15, n-1 jackknife resampling tests are plotted against the temporal-profile (light teal background), spatial-profile (teal background), and noise-correlation (dark teal background) measures. Horizontal dashed lines demarcate the significance level. Red squares indicate that the test statistics were significant throughout all tests. (For interpretation of the references to color in this figure legend, the reader is referred to the Web version of this article.)

stimulus- or task-driven neural responses in the non-visual cortices in animals and humans, including the somatosensory cortex of rats [1,46], the motor cortex of cats [2], the hippocampal slices of rats [47], and the motor cortex of humans [48,49]. By contrast, the current-induced modulation of the stimulus-driven responses was much weaker in the visual cortex than in the motor cortex while the spontaneous responses were equally pronounced in the two cortices [2]. For that matter, the dissociation between baseline and stimulus-driven BOLD responses in our data appears to mirror the observed differences in the visual cortex.

Nevertheless, it should be noted that the direction of the applied electric current relative to the cortical surface is one of the key factors determining the efficacy of tDCS [50–54]. In this regard, the difference in tDCS effects on stimulus- or task-driven BOLD responses between the visual and motor cortices could have resulted from the differences in cortical folding structure.

4.3. *A-tDCS sharpens the spatial tuning of pRF by augmenting surround suppression*

Visual neurons are known to be suppressed by the visual input presented in the surround of its receptive field, a phenomenon called 'surround suppression' ([55–58]; see Ref. [59]). The surround suppression is explained by the divisive normalization model, in which the surround exerts a divisive, inhibitory influence on the responses to the center [55,

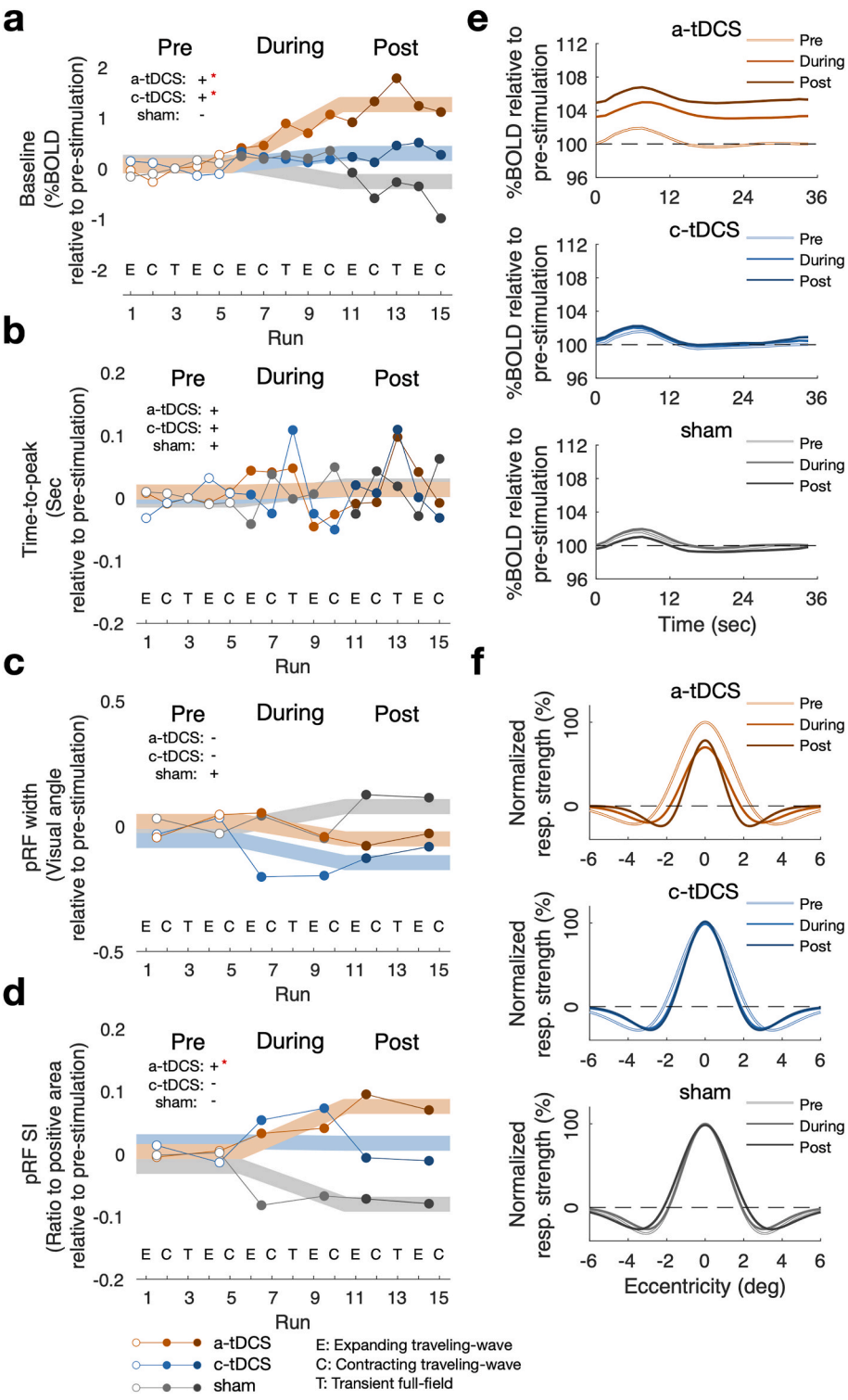

Fig. 6. Time courses and illustrative summary of the principal tDCS effects.
(a-d) Across-run changes of baseline (a), time-to-peak (b), pRF width (c), and pRF SI (d) measures for a-tDCS (red), c-tDCS (blue), and sham-tDCS (gray) sessions. Across-voxel averages of the measures are plotted as a function of scan runs for each daily session. The measures were adapted to their own averages during the pre-stimulation phase. Dots and thin lines are the time courses of the data, whereas thick lines are those of the regression models, the signs and significances of which are indicated in the upper left corner of each panel (*: $p < 0.05$). Letters at the bottom denote the scan type: E and C for expanding and contracting traveling-wave input scans, respectively; T for transient whole-field input scans. (e–f) Illustrative summary of tDCS effects on BOLD responses to the transient full-field input (e) and pRF shapes (f). The plots summarize the results from a subset of voxels that showed the effects consistent with the grand average effects for all the following measures during the post-stimulation phase: 'baseline', 'time-to-peak', 'pRF width', and 'pRF SI'. Panels correspond to daily sessions, indicated by the corresponding colors of plotted curves. (For interpretation of the references to color in this figure legend, the reader is referred to the Web version of this article.)

60]. The pRF-estimation models based on the DoG function or its variants have incorporated those configurations in mapping the spatial tuning functions of single fMRI voxels [44,61]. The pRF models fit to BOLD responses tightly reflected the center-surround configurations measured by the multi-unit activity [62].

Based on the above rationale, the a-tDCS-induced increase of SI in our study suggests that a-tDCS augments the surround suppression in the visual cortex, which consequently sharpens the spatial tuning of visual neurons. Thus, our findings offer an account of the a-tDCS-induced improvement in human visual acuity, a phenomenon considered counterintuitive [63]. According to our interpretation, the augmented inhibitory influence from the suppressive surround narrows the spatial tuning curve of visual neurons, conferring the visual system with precise sensory encoding [64].

4.4. *Possible neural mechanisms for tDCS effects on EVC*

The most potent yet intriguing effects of a-tDCS in our study are the simultaneous buildup and persistence of the baseline—but not stimulus-driven—BOLD activity and the surround suppression. What neural

mechanism(s) mediates the co-existence of these seemingly counteracting effects? Why does a-tDCS not elevate stimulus-driven BOLD responses in the early visual cortex? We address these questions by relating the hierarchical gradients in excitatory and inhibitory recurrent connections [65] to the neural metabolism underlying BOLD responses [66]. In brief, we conjecture that a-tDCS to the primate visual cortex preferentially increases synaptic inhibition by upregulating the activity of a subtype(s) of GABAergic cells in the recurrent connections, which increases the local brain metabolism leading to an increase in net BOLD activity.

Recent large-scale investigations on the biophysical properties of primate brains, including humans, revealed that the recurrent connections systematically vary along the hierarchy of cortical areas in two critical aspects. First, the number of spines on pyramidal dendrites—a proxy of synaptic excitation strength—steeply increases along the hierarchy, being lowest in the early visual cortex, intermediate in the motor cortex, and highest in the prefrontal cortex [23]. Second, the relative proportions of subtype GABAergic interneurons vary along the hierarchy: those inhibiting the synaptic input to excitatory neurons are most dominant in the early visual cortex, whereas those inhibiting excitatory neurons' output become increasingly dominant along the hierarchy [24].

These "hierarchical gradients" [65] imply that a-tDCS is likely to cause different outcomes in recurrent neural activity depending on the cortical site of stimulation. The effects of a-tDCS in our study might have to do with the extreme position of the early visual cortex on the gradients of recurrent connections. It is likely that a-tDCS in the early visual cortex preferentially up-regulates the contribution of the synaptic-inhibition-controlling type of GABAergic neurons to the E/I balanced network. Then, this can account for the a-tDCS-induced augmentation of surround suppression. Next, unlike the output-controlling type of GABAergic neurons, the synaptic-inhibition-controlling type of GABAergic neurons consume metabolic energy substantially so that its energy consumption overcomes the decrease of metabolic consumption due to spiking reduction [67,68]. Then, this can account for the a-tDCS-induced increase in baseline BOLD activity.

The scenario presented above is only a speculative and *ad hoc* account. Nonetheless, it is critical to consider the substantial differences in E/I balanced network composition across different cortical areas when interpreting any given effects of tDCS. Such considerations will make tDCS an effective tool for investigating the circuit-level neural mechanisms responsible for major psychiatric diseases such as Schizophrenia. For instance, the previously reported weak surround suppression in schizophrenic patients [69,70] might be enhanced by a-tDCS on their visual cortex, which can be an exciting future extension of the current work.

4.5. Issues with the use of high-definition tDCS

To effectively stimulate EVC, our target cortical region, we employed multi-channel high-definition tDCS (HD-tDCS), which provides higher focality and density of electric fields than the conventional tDCS [71–73]. However, this increased focality may invite unwanted inter-individual variability [73]. Hence, as recommended by Ref. [73], we optimized the injection current pattern for each individual's brain based on the sophisticated FE head model constructed from T1-weighted MR images. Despite this effort, inter-individual variability in tDCS efficacy cannot be completely avoided due to differences in various aspects [6,7], including brain and skull morphology. Our analysis indeed showed that the electric-field intensity delivered to EVC was correlated with the distance from the central electrode to EVC (Fig. 1e). We also found that the changes in baseline BOLD increased as a function of electric-field intensity (Supplementary Fig. 1.), which further confirms that the changes in baseline BOLD can be ascribed to a-tDCS. To statistically address any inter-individual variability in tDCS efficacy remaining after our current optimization procedure, we adopted the mixed-effect model, treating "subject" as a random variable, and conducted the jackknife resampling analysis (Fig. 5). However, to fully assess the inter-individual variability associated with the use of HD-tDCS, it would be best to confirm our findings with a larger sample size.

In our study, we did not observe the expected polarity effect between a-tDCS and c-tDCS. While previous research has already debunked the classic polarity effect [3], our null result for c-tDCS could be attributed to our use of HD-tDCS. The multiple electrodes in a center-surround configuration may not align with the traditional definitions of "anodal" and "cathodal" [74,75]. Therefore, caution should be exercised in interpreting the null effect of c-tDCS in our study, especially when applying the conventional understanding of tDCS polarity effects.

CRediT authorship contribution statement

Jeongyeol Ahn: Conceptualization, Methodology, Software, Validation, Formal analysis, Investigation, Data curation, Writing – original draft, Visualization. **Juhyoung Ryu:** Conceptualization, Methodology, Investigation, Data curation. **Sangjun Lee:** Methodology, Software, Formal analysis, Data curation. **Chany Lee:** Methodology, Software, Formal analysis, Data curation, Writing – original draft. **Chang-Hwan Im:** Writing – review & editing, Supervision, Project administration. **Sang-Hun Lee:** Conceptualization, Resources, Writing – review & editing, Supervision, Project administration, Funding acquisition.

Declaration of competing interest

The authors declare that they have no known competing financial interests or personal relationships that could have influenced the work reported in this paper.

Acknowledgements

This research was supported by the Seoul National University Research Grant 339-20220013 and by the Brain Research Program through the National Research Foundation of Korea (NRF) funded by the Ministry of Science and Information and Communications Technology Grant No. NRF-2021R1F1A1052020.

Appendix A. Supplementary data

Supplementary data to this article can be found online at https://doi.org/10.1016/j.brs.2023.07.052.

References

[1] Bindman LJ, Lippold OCJ, Redfearn JWT. The action of brief polarizing currents on the cerebral cortex of the rat (1) during current flow and (2) in the production of long-lasting after-effects. J Physiol 1964;172:369–82. https://doi.org/10.1113/jphysiol.1964.sp007425.

[2] Creutzfeldt OD, Fromm GH, Kapp H. Influence of transcortical d-c currents on cortical neuronal activity. Exp Neurol 1962;5:436–52. https://doi.org/10.1016/0014-4886(62)90056-0.

[3] Wiethoff S, Hamada M, Rothwell JC. Variability in response to transcranial direct current stimulation of the motor cortex. Brain Stimul 2014;7:468–75. https://doi.org/10.1016/j.brs.2014.02.003.

[4] Jacobson L, Koslowsky M, Lavidor M. tDCS polarity effects in motor and cognitive domains: a meta-analytical review. Exp Brain Res 2012;216:1–10. https://doi.org/10.1007/s00221-011-2891-9.

[5] Esmaeilpour Z, Shereen AD, Ghobadi-Azbari P, Datta A, Woods AJ, Ironside M, et al. Methodology for tDCS integration with fMRI. Hum Brain Mapp 2020;41:1950–67. https://doi.org/10.1002/hbm.24908.

[6] Li LM, Uehara K, Hanakawa T. The contribution of interindividual factors to variability of response in transcranial direct current stimulation studies. Front Cell Neurosci 2015;9:181. https://doi.org/10.3389/fncel.2015.00181.

[7] Vergallito A, Feroldi S, Pisoni A, Romero Lauro LJ. Inter-individual variability in tDCS effects: a narrative review on the contribution of stable, variable, and contextual factors. Brain Sci 2022;12. https://doi.org/10.3390/brainsci12050522.

[8] Molaee-Ardekani B, Márquez-Ruiz J, Merlet I, Leal-Campanario R, Gruart A, Sánchez-Campusano R, et al. Effects of transcranial Direct Current Stimulation (tDCS) on cortical activity: a computational modeling study. Brain Stimul 2013;6:25–39. https://doi.org/10.1016/j.brs.2011.12.006.

[9] Kim J-H, Kim D-W, Chang WH, Kim Y-H, Kim K, Im C-H. Inconsistent outcomes of transcranial direct current stimulation may originate from anatomical differences among individuals: electric field simulation using individual MRI data. Neurosci Lett 2014;564:6–10. https://doi.org/10.1016/j.neulet.2014.01.054.

[10] Laakso I, Mikkonen M, Koyama S, Hirata A, Tanaka S. Can electric fields explain inter-individual variability in transcranial direct current stimulation of the motor cortex? Sci Rep 2019;9:626. https://doi.org/10.1038/s41598-018-37226-x.

[11] Brunoni AR, Kemp AH, Shiozawa P, Cordeiro Q, Valiengo LCL, Goulart AC, et al. Impact of 5-HTTLPR and BDNF polymorphisms on response to sertraline versus transcranial direct current stimulation: implications for the serotonergic system. Eur Neuropsychopharmacol 2013;23:1530–40. https://doi.org/10.1016/j.euroneuro.2013.03.009.

[12] Woods AJ, Antal A, Bikson M, Boggio PS, Brunoni AR, Celnik P, et al. A technical guide to tDCS, and related non-invasive brain stimulation tools. Clin Neurophysiol 2016;127:1031–48. https://doi.org/10.1016/j.clinph.2015.11.012.

[13] Hubel DH, Wiesel TN. Receptive fields and functional architecture of monkey striate cortex. J Physiol 1968;195:215–43. https://doi.org/10.1113/jphysiol.1968.sp008455.

[14] Carandini M, Demb JB, Mante V, Tolhurst DJ, Dan Y, Olshausen BA, et al. Do we know what the early visual system does? J Neurosci 2005;25:10577. https://doi.org/10.1523/JNEUROSCI.3726-05.2005.

[15] Lennie P, Movshon JA. Coding of color and form in the geniculostriate visual pathway (invited review). J Opt Soc Am A 2005;22:2013–33. https://doi.org/10.1364/JOSAA.22.002013.

[16] Nassi JJ, Callaway EM. Parallel processing strategies of the primate visual system. Nat Rev Neurosci 2009;10:360–72. https://doi.org/10.1038/nrn2619.

[17] Stagg CJ, O'Shea J, Kincses ZT, Woolrich M, Matthews PM, Johansen-Berg H. Modulation of movement-associated cortical activation by transcranial direct current stimulation. Eur J Neurosci 2009;30:1412–23. https://doi.org/10.1111/j.1460-9568.2009.06937.x.

[18] Jang SH, Ahn SH, Byun WM, Kim CS, Lee MY, Kwon YH. The effect of transcranial direct current stimulation on the cortical activation by motor task in the human brain: an fMRI study. Neurosci Lett 2009;460:117–20. https://doi.org/10.1016/j.neulet.2009.05.037.

[19] Kim CR, Kim D-Y, Kim LS, Chun MH, Kim SJ, Park CH. Modulation of cortical activity after anodal transcranial direct current stimulation of the lower limb motor cortex: a functional MRI study. Brain Stimul 2012;5:462–7. https://doi.org/10.1016/j.brs.2011.08.002.

[20] Kwon YH, Ko M-H, Ahn SH, Kim Y-H, Song JC, Lee C-H, et al. Primary motor cortex activation by transcranial direct current stimulation in the human brain. Neurosci Lett 2008;435:56–9. https://doi.org/10.1016/j.neulet.2008.02.012.

[21] Baudewig J, Nitsche MA, Paulus W, Frahm J. Regional modulation of BOLD MRI responses to human sensorimotor activation by transcranial direct current stimulation. Magn Reson Med 2001;45:196–201. https://doi.org/10.1002/1522-2594(200102)45:2<196::AID-MRM1026>3.0.CO;2-1.

[22] Antal A, Polania R, Schmidt-Samoa C, Dechent P, Paulus W. Transcranial direct current stimulation over the primary motor cortex during fMRI. Neuroimage 2011;55:590–6. https://doi.org/10.1016/j.neuroimage.2010.11.085.

[23] Chaudhuri R, Knoblauch K, Gariel M-A, Kennedy H, Wang X-J. A large-scale circuit mechanism for hierarchical dynamical processing in the primate cortex. Neuron 2015;88:419–31. https://doi.org/10.1016/j.neuron.2015.09.008.

[24] Wang X-J. The prefrontal lobes: development, function and pathology. Front. Lobes Dev. Funct. Pathol. 2006:92–127. Cambridge University Press.

[25] Engel SA, Rumelhart DE, Wandell BA, Lee AT, Glover GH, Chichilnisky E-J, et al. fMRI of human visual cortex. Nature 1994;369:525. https://doi.org/10.1038/369525a0. 525.

[26] Kay KN, Naselaris T, Prenger RJ, Gallant JL. Identifying natural images from human brain activity. Nature 2008;452:352–5. https://doi.org/10.1038/nature06713.

[27] Naselaris T, Prenger RJ, Kay KN, Oliver M, Gallant JL. Bayesian reconstruction of natural images from human brain activity. Neuron 2009;63:902–15. https://doi.org/10.1016/j.neuron.2009.09.006.

[28] Thirion B, Duchesnay E, Hubbard E, Dubois J, Poline J-B, Lebihan D, et al. Inverse retinotopy: inferring the visual content of images from brain activation patterns. Neuroimage 2006;33:1104–16. https://doi.org/10.1016/j.neuroimage.2006.06.062.

[29] Kriegeskorte N. Deep neural networks: a new framework for modeling biological vision and brain information processing. Annu Rev Vis Sci 2015;1:417–46. https://doi.org/10.1146/annurev-vision-082114-035447.

[30] Weliky M, Kandler K, Fitzpatrick D, Katz LC. Patterns of excitation and inhibition evoked by horizontal connections in visual cortex share a common relationship to orientation columns. Neuron 1995;15:541–52. https://doi.org/10.1016/0896-6273(95)90143-4.

[31] Somers DC, Todorov EV, Siapas AG, Toth LJ, Kim DS, Sur M. A local circuit approach to understanding integration of long-range inputs in primary visual cortex. Cerebr Cortex 1998;8:204–17. https://doi.org/10.1093/cercor/8.3.204.

[32] Tremblay R, Lee S, Rudy B. GABAergic interneurons in the neocortex: from cellular properties to circuits. Neuron 2016;91:260–92. https://doi.org/10.1016/j.neuron.2016.06.033.

[33] Adesnik H, Bruns W, Taniguchi H, Huang ZJ, Scanziani M. A neural circuit for spatial summation in visual cortex. Nature 2012;490:226–31. https://doi.org/10.1038/nature11526.

[34] Averbeck BB, Latham PE, Pouget A. Neural correlations, population coding and computation. Nat Rev Neurosci 2006;7:358–66. https://doi.org/10.1038/nrn1888.

[35] Cohen MR, Kohn A. Measuring and interpreting neuronal correlations. Nat Neurosci 2011;14:811–9. https://doi.org/10.1038/nn.2842.

[36] Ryu J, Lee S-H. Stimulus-tuned structure of correlated fMRI activity in human visual cortex. Cerebr Cortex 2017;28:693–712. https://doi.org/10.1093/cercor/bhw411.

[37] van Bergen RS, Jehee JFM. Modeling correlated noise is necessary to decode uncertainty. New Adv Encoding Decod Brain Signals 2018;180:78–87. https://doi.org/10.1016/j.neuroimage.2017.08.015.

[38] Zhang R-Y, Wei X-X, Kay K. Understanding multivariate brain activity: evaluating the effect of voxelwise noise correlations on population codes in functional magnetic resonance imaging. PLoS Comput Biol 2020;16:e1008153. https://doi.org/10.1371/journal.pcbi.1008153.

[39] Fischl B. FreeSurfer. NeuroImage 2012;62:774–81. https://doi.org/10.1016/j.neuroimage.2012.01.021.

[40] Jenkinson M, Beckmann CF, Behrens TEJ, Woolrich MW, Smith SM. Fsl. NeuroImage 2012;62:782–90. https://doi.org/10.1016/j.neuroimage.2011.09.015.

[41] Thielscher A, Antunes A, Saturnino GB. Field modeling for transcranial magnetic stimulation: a useful tool to understand the physiological effects of TMS?. In: Proc annu int conf IEEE eng med biol soc EMBS; 2015. https://doi.org/10.1109/EMBC.2015.7318340. 2015-Novem:222–5.

[42] Lotte F, Bougrain L, Clerc M. Electroencephalography (EEG)-Based brain-computer interfaces. Wiley encycl. Electr. Electron. Eng. Hoboken, NJ, USA: John Wiley & Sons, Inc.; 2015. p. 1–20. https://doi.org/10.1002/047134608X.W8278.

[43] Glover GH. Deconvolution of impulse response in event-related BOLD fMRI1. Neuroimage 1999;9:416–29. https://doi.org/10.1006/nimg.1998.0419.

[44] Zuiderbaan W, Harvey BM, Dumoulin SO. Modeling center–surround configurations in population receptive fields using fMRI. J Vis 2012;12:10. https://doi.org/10.1167/12.3.10. 10.

[45] Fisher RA. On the "probable error" of a coefficient of correlation deduced from a small sample. Metron 1921;1:1–32.

[46] Bindman LJ, Lippold OCJ, Redfearn JWT. Long-lasting changes in the level of the electrical activity of the cerebral cortex produced by polarizing currents. Nature 1962;196:584–5. https://doi.org/10.1038/196584a0.

[47] Bikson M, Inoue M, Akiyama H, Deans JK, Fox JE, Miyakawa H, et al. Effects of uniform extracellular DC electric fields on excitability in rat hippocampal slices in vitro. J Physiol 2004;557:175–90. https://doi.org/10.1113/jphysiol.2003.055772.

[48] Nitsche MA, Paulus W. Excitability changes induced in the human motor cortex by weak transcranial direct current stimulation. J Physiol 2000;527:633–9. https://doi.org/10.1111/j.1469-7793.2000.t01-1-00633.x.

[49] Nitsche MA, Paulus W. Sustained excitability elevations induced by transcranial DC motor cortex stimulation in humans. Neurology 2001;57:1899. https://doi.org/10.1212/WNL.57.10.1899.

[50] Evans C, Zich C, Lee JSA, Ward N, Bestmann S. Inter-individual variability in current direction for common tDCS montages. Neuroimage 2022;260:119501. https://doi.org/10.1016/j.neuroimage.2022.119501.

[51] Farahani F, Kronberg G, FallahRad M, Oviedo HV, Parra LC. Effects of direct current stimulation on synaptic plasticity in a single neuron. Brain Stimul 2021;14:588–97. https://doi.org/10.1016/j.brs.2021.03.001.

[52] Paulus W, Antal A, Nitsche MA. 4 physiological basis and methodological aspects of transcranial. Transcranial Brain Stimul 2012;93.

[53] Seo H, Jun SC. Relation between the electric field and activation of cortical neurons in transcranial electrical stimulation. Brain Stimul 2019;12:275–89. https://doi.org/10.1016/j.brs.2018.11.004.

[54] Rahman A, Lafon B, Bikson M. Chapter 2 - multilevel computational models for predicting the cellular effects of noninvasive brain stimulation. In: Bestmann S, editor. Prog. Brain res., vol. 222. Elsevier; 2015. p. 25–40. https://doi.org/10.1016/bs.pbr.2015.09.003.

[55] Cavanaugh JR, Bair W, Movshon JA. Selectivity and spatial distribution of signals from the receptive field surround in macaque V1 neurons. J Neurophysiol 2002;88:2547–56. https://doi.org/10.1152/jn.00693.2001.

[56] Cavanaugh JR, Bair W, Movshon JA. Nature and interaction of signals from the receptive field center and surround in macaque V1 neurons. J Neurophysiol 2002;88:2530–46. https://doi.org/10.1152/jn.00692.2001.

[57] Kapadia MK, Westheimer G, Gilbert CD. Dynamics of spatial summation in primary visual cortex of alert monkeys. Proc Natl Acad Sci USA 1999;96:12073. https://doi.org/10.1073/pnas.96.21.12073. 8.

[58] Sceniak MP, Ringach DL, Hawken MJ, Shapley R. Contrast's effect on spatial summation by macaque V1 neurons. Nat Neurosci 1999;2:733–9. https://doi.org/10.1038/11197.

[59] Carandini M. Receptive fields and suppressive fields in the early visual system. Cognit Neurosci 2004;3:313–26.

[60] Carandini M, Heeger DJ. Normalization as a canonical neural computation. Nat Rev Neurosci 2012;13:51–62. https://doi.org/10.1038/nrn3136.

[61] Aqil M, Knapen T, Dumoulin SO. Divisive normalization unifies disparate response signatures throughout the human visual hierarchy. Proc Natl Acad Sci USA 2021;118:e2108713118. https://doi.org/10.1073/pnas.2108713118.

[62] Klink PC, Chen X, Vanduffel W, Roelfsema PR. Population receptive fields in nonhuman primates from whole-brain fMRI and large-scale neurophysiology in visual cortex. Elife 2021;10:e67304. https://doi.org/10.7554/eLife.67304.

[63] Reinhart RMG, Xiao W, McClenahan LJ, Woodman GF. Electrical stimulation of visual cortex can immediately improve spatial vision. Curr Biol 2016;26:1867–72. https://doi.org/10.1016/j.cub.2016.05.019.

[64] Schoups A, Vogels R, Qian N, Orban G. Practising orientation identification improves orientation coding in V1 neurons. Nature 2001;412:549–53. https://doi.org/10.1038/35087601.
[65] Wang X-J. Macroscopic gradients of synaptic excitation and inhibition in the neocortex. Nat Rev Neurosci 2020;21:169–78. https://doi.org/10.1038/s41583-020-0262-x.
[66] Logothetis NK. What we can do and what we cannot do with fMRI. Nature 2008;453:869–78. https://doi.org/10.1038/nature06976.
[67] Ackermann R, Finch D, Babb T, Engel J. Increased glucose metabolism during long-duration recurrent inhibition of hippocampal pyramidal cells. J Neurosci 1984;4:251. https://doi.org/10.1523/JNEUROSCI.04-01-00251.1984.
[68] Nudo RJ, Masterton RB. Stimulation-induced [14C]2-deoxyglucose labeling of synaptic activity in the central auditory system. J Comp Neurol 1986;245:553–65. https://doi.org/10.1002/cne.902450410.
[69] Dakin S, Carlin P, Hemsley D. Weak suppression of visual context in chronic schizophrenia. Curr Biol 2005;15:R822–4. https://doi.org/10.1016/j.cub.2005.10.015.
[70] Serrano-Pedraza I, Romero-Ferreiro V, Read JCA, Diéguez-Risco T, Bagney A, Caballero-González M, et al. Reduced visual surround suppression in schizophrenia shown by measuring contrast detection thresholds. Front Psychol 2014;5:1431. https://doi.org/10.3389/fpsyg.2014.01431.
[71] Edwards D, Cortes M, Datta A, Minhas P, Wassermann EM, Bikson M. Physiological and modeling evidence for focal transcranial electrical brain stimulation in humans: a basis for high-definition tDCS. Neuroimage 2013;74:266–75. https://doi.org/10.1016/j.neuroimage.2013.01.042.
[72] Hill AT, Rogasch NC, Fitzgerald PB, Hoy KE. Effects of prefrontal bipolar and high-definition transcranial direct current stimulation on cortical reactivity and working memory in healthy adults. Neuroimage 2017;152:142–57. https://doi.org/10.1016/j.neuroimage.2017.03.001.
[73] Kuo H-I, Bikson M, Datta A, Minhas P, Paulus W, Kuo M-F, et al. Comparing cortical plasticity induced by conventional and high-definition 4 × 1 ring tDCS: a neurophysiological study. Brain Stimul 2013;6:644–8. https://doi.org/10.1016/j.brs.2012.09.010.
[74] Masina F, Arcara G, Galletti E, Cinque I, Gamberini L, Mapelli D. Neurophysiological and behavioural effects of conventional and high definition tDCS. Sci Rep 2021;11:7659. https://doi.org/10.1038/s41598-021-87371-z.
[75] Garnett EO, Malyutina S, Datta A, den Ouden D-B. On the use of the terms anodal and cathodal in high-definition transcranial direct current stimulation: a technical note. Neuromod Technol Neural Interface 2015;18:705–13. https://doi.org/10.1111/ner.12320.